INFLUENCE OF STRESS ON ELASTIC WAVE VELOCITY AROUND A BOREHOLE IN ROCKS

Jiayong TIAN [1], Yuanpeng MAN [2], Zhoumin XIE [1], and Hui QI [2]

[1] *Institute of Crustal Dynamics, CEA, Subbox 28, Beijing P.O.Box 2855, Beijing, P.R.China, 100085*
[2] *Harbin Engineering University, Harbin, P.R.China, 150001*
Email: chenlitedtian@yahoo.com.cn

ABSTRACT :

In this paper, we introduce acoustoelasticity theory to investigate wave-velocity distribution and polarization around a borehole in prestressed rocks to build their direct and explicit link macroscopically. The acoustoelasticity theory based on non-linear continuum mechanics invokes third-order elastic constants to explain the stress-induced wave-velocity change of rocks. The numerical results show that directions of the maximum and minimum wave-velocity change around a borehole correspond to those of the minimum and maximum far-field principal rock stresses, respectively. In order to validate the theoretical analysis, wave velocities around a borehole in sand stone under the biaxial loading are measured by pulse-echo method. The detail discussion shows that the experimental results coincide with the theoretical results, which means that the ultrasonic method based on acoustoelasticity theory could be a promising measurement method for in-situ rock stresses.

KEYWORDS: Acoustoelasticity, In-situ stress, Ultrasonic waves, Rock, Wave velocity

1.INTRODUCTION

Many experimental observations have shown that the existence of initial stress in metal materials yields elastic anisotropy and then shear-wave splitting, which is known as acoustoelasticity birefringence. [1] Acoustoelasticity theory had been developed to explain these phenomena, which has been widely used in the measurements of residual stress, plastic damage, and plastic strain ratio of metal materials. [2] In rock engineering, the stress-induced shear-wave splitting also appears in rocks, at the same time, the sensitivity of wave velocity to rock stresses is much more than metal materials.[3] Johnson and Rasolofosan [4] verified that stress-induced anisotropy of P wave for rocks is much more than acoustoelasticity birefringence. Huang et al. [5] demonstrated that the acoustoelasticity theory for the metal materials could interpret the experimental results of rocks effectively. Vega [6] discussed the difference between wave-velocity anisotropy induced by intrinsic anisotropy and the initial stresses. Winkler et al. [7] studied the influence of stress concentration in sonic logging on acoustic-wave velocity, which shows that the initial rock stresses lead to crossover of dispersive curve but intrinsic anisotropy of rock not. Sinha et al. [8] investigated the effect of three-axial stresses on the dispersion of Stoneley wave and flexural wave, and indicated that the polarization direction of fast shear wave coincides with that of maximum far-field principal stresses and the shear-wave anisotropy is proportional to the stress magnitude. All above mentioned show that the rock stresses have great influence on wave velocity.

Since the in-situ stress measurement in the tunnel of Hoover dam in 1932，hydraulic fracture method, stress relief method, and acoustic emission method have been developed to measure in-situ rock stresses.[9,10] As a direct method, hydraulic fracture method must be satisfied that the directions of one principal stresses coincide with that of borehole axis and no micro-crack exists in the rock. Acoustic emission method being based on Kaiser effect of rocks, is related with not only modern stresses but also historical stresses. Stress-relief method uses the strain-meter to measure surface strains of the borehole and then the stresses. The sensor element does not measure the surface strain directly, which needs the calibration before each measurement. The present measurement methods for in-situ rock stresses have evident error and high expense. However, the high-resolution and convenient measurement of wave velocity promises quantitative evaluation of in-situ rock stresses from the measurement of the wave-velocity changes for rocks conveniently.

In this paper, we investigate the quantitative acoustoelastic relation around a rock borehole based on the acoustoelasticity theory of the continuum. First, we introduce acoustoelasticity theory of rocks briefly, and then

combine the strain and stress fields around a borehole to investigate the quantitative acoustoelasticity around a borehole of rock mass. Second, in order to verify the theoretical results, pulse-echo method is adopted to measure the velocity changes of longitudinal wave and shear waves around a borehole subjected to far-field bi-axial stresses. The numerical and experimental results show that the acoustoelasticity theory of the continuum is applicable for measuring the in-situ rock stresses.

2.ACOUSTOELASTICITY THEORY OF ROCK

Based on the non-linear continuum mechanics, the acoustoelasticity theory of rock is introduced to establish a theoretical basis for stress-induced wave-velocity change of rocks, which considers the large deformation and the nonlinear stress-strain relation of rock. There exist natural state, initial state, and final state in acoustoelasticity theory of rock. The natural state is the state where a rock is in the original state free of stress and strain, and the initial state if a rock has been deformed or under the action of applied loading. When a dynamic disturbance is superimposed on the rock in the initial state, the rock is further deformed to the final state. Physical variables in the natural, initial, or final states are denoted by a superscript label *0*, *i*, or *f*, respectively. The position of a particle in the rock at natural, initial, and final states are measured by ξ, **X**, and **x**, respectively. The components of ξ and other physical quantities which refer to the natural configuration are denoted by Greek subscripts.
Assumptions of the initial static deformation, small dynamic disturbance, and hyperelastic constitutive equation yield the equation of motion for displacements $\mathrm{u}(\xi,t)$ caused by the dynamic disturbance with reference to the natural coordinate [1]

$$\frac{\partial}{\partial \xi_\beta}\left[T^i_{\gamma\beta}\frac{\partial u_\alpha}{\partial \xi_\gamma}+\Gamma_{\alpha\beta\gamma\delta}\frac{\partial u_\gamma}{\partial \xi_\delta}\right]=\rho_0\ddot{u}_\alpha \tag{1}$$

where $T^i_{\alpha\beta}$ and $e^i_{\alpha\beta}$ are the initial static stresses and strains, respectively. ρ_0 is the mass density of the rock. $\Gamma_{\alpha\beta\gamma\delta}=c_{\alpha\beta\gamma\delta}+c_{\alpha\beta\gamma\delta\zeta\eta}\frac{\partial u^i_\gamma}{\partial \zeta_\lambda}+c_{\lambda\beta\gamma\delta}\frac{\partial u^i_\alpha}{\partial \zeta_\lambda}+c_{\alpha\beta\gamma\delta\zeta\eta}e^i_{\zeta\eta}$. $c_{\alpha\beta\gamma\delta}$ and $c_{\alpha\beta\gamma\delta\zeta\eta}$ are the second-order elastic constants and the third-order elastic constants, respectively. For isotropic elastic solid, there exist two independent second-order elastic constants (Lame constants λ and μ) and three independent third-order elastic constants (Murnaghan constants l, m, and n) [11].

3. QUANTITATIVE ACOUSTOELASTICITY RELATION AROUND A BOREHOLE

Considering a borehole of radius a in an infinite, homogeneous, isotropic rock subjected to far-field principal stresses σ_{11}, σ_{22}, and σ_{33} shown in Fig.1, we define a Cartesian coordinate system (x,y,z) and a cylindrical coordinate system (r,θ,z) with coincident origin and z axis, which coincides with the borehole axis. Here we assume that the elastic waves propagate along the borehole axis.

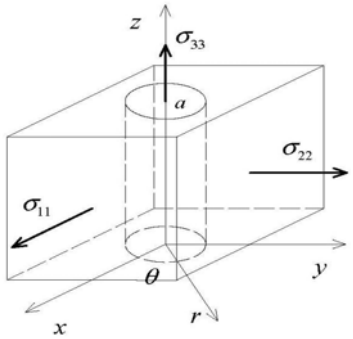

Fig.1 Mechanical model of a borehole in an infinite, homogeneous, isotropic rock under the far-field principal stresses.

Eq. (1) shows that if the quantitative acoustoelastic relation around a borehole can be deduced, the displacements and stresses around a borehole induced by far-field stresses must be provided.

a) ***Displacements and stresses around a borehole subjected to far-field stresses***

According to the linear elasticity, the displacements around a borehole in an infinite rock subjected to far-field principal stresses σ_{11}, σ_{22}, and σ_{33} are expressed as [9]

$$u_r^i(r,\theta)=\frac{(1+\nu)}{E}\left\{\begin{array}{l}\left[\frac{(1-\nu)(\sigma_{11}+\sigma_{22})}{2(1+\nu)}-\frac{\nu}{(1+\nu)}\sigma_{33}\right]r+\frac{(\sigma_{11}+\sigma_{22})a^2}{2r}\\ +r\left[1-\frac{a^4}{r^4}+\frac{4(1-\nu)a^2}{r^2}\right]\left[\frac{(\sigma_{11}-\sigma_{22})\cos(2\theta)}{2}\right]\end{array}\right\} \tag{2}$$

$$u_\theta^i(r,\theta)=\frac{(1+\nu)}{E}\left[-r-\frac{a^4}{r^3}-\frac{2(1-2\nu)a^2}{r}\right]\left[\frac{(\sigma_{11}-\sigma_{22})\sin(2\theta)}{2}\right] \tag{3}$$

$$u_z^i(r,\theta,z)=\frac{(1+\nu)}{E}\left[\frac{z\sigma_{33}}{1+\nu}-\frac{\nu z(\sigma_{11}+\sigma_{22})}{(1+\nu)}\right] \tag{4}$$

where E and ν are Young's modulus and Poisson ratio of rocks, respectively. The stresses around a borehole are denoted by

$$T_{rr}^i(r,\theta)=\frac{(\sigma_{11}+\sigma_{22})}{2}(1-\frac{a^2}{r^2})+\frac{(\sigma_{11}-\sigma_{22})}{2}(1+\frac{3a^4}{r^4}-\frac{4a^2}{r^2})\cos(2\theta) \tag{5}$$

$$T_{\theta\theta}^i(r,\theta)=\frac{(\sigma_{11}+\sigma_{22})}{2}(1+\frac{a^2}{r^2})-\frac{(\sigma_{11}-\sigma_{22})}{2}(1+\frac{3a^4}{r^4})\cos(2\theta) \tag{6}$$

$$T_{zz}^i=-\frac{2\nu(\sigma_{11}-\sigma_{22})a^2\cos(2\theta)}{r^2}+\sigma_{33} \tag{7}$$

$$T_{r\theta}^i=-\frac{(\sigma_{11}-\sigma_{22})}{2}(1-\frac{3a^4}{r^4}+\frac{2a^2}{r^2})\sin(2\theta) \tag{8}$$

$$T_{\theta z}^i=T_{rz}^i=0 \tag{9}$$

The above equations show that stress concentration around a borehole decreases with the increase of the distance far from the borehole surface. When the distance far from the borehole surface is one and a half time greater than the borehole radius, the influence of borehole on the far-filed stress fields can be ignored.

b) The plane waves propagating along the borehole axis

A plane harmonic wave propagating along the borehole axis is considered, whose displacements are represented in cylindrical coordinate as

$$\left.\begin{array}{l}u_r(r,\theta,z)=\left[u_{r0}\cos(\theta-\alpha_0)+u_{\theta 0}\sin(\theta-\alpha_0)\right]\exp(\mathrm{i}kz-\mathrm{i}\omega t)\\ u_\theta(r,\theta,z)=\left[-u_{r0}\sin(\theta-\alpha_0)+u_{\theta 0}\cos(\theta-\alpha_0)\right]\exp(\mathrm{i}kz-\mathrm{i}\omega t)\\ u_z(r,\theta,z)=u_{z0}\exp(\mathrm{i}kz-\mathrm{i}\omega t)\end{array}\right\} \tag{10}$$

where u_{r0}, $u_{\theta 0}$, and u_{z0} are unknown amplitudes, ω the angular frequency, k wave number, α_0 is the angle made by polarization of shear waves to the x_1 axis. Substitution of Eqs. (2)-(10) into expressions of Eq. (1) in cylindrical coordinate, and then letting $\theta=\alpha_0$ give rise to a system of equations for the unknown amplitude

$$\begin{bmatrix} S_{11}+R_{11}^{d}D & S_{12}+R_{12}^{d}D & S_{13} \\ S_{21}+R_{21}^{d}D & S_{22}+R_{22}^{d}D & S_{23} \\ S_{31} & S_{32} & S_{33}+R_{33}^{d}D \end{bmatrix} \begin{bmatrix} u_{r0} \\ u_{\theta 0} \\ u_{z0} \end{bmatrix} = 0 \tag{11}$$

where $D = V/\sqrt{\mu/\rho}$ is normalized wave velocity related with shear waves. The coefficients in the characteristic equation are given in Appendix. Polarization of shear waves can be given by the eigenvectors. Eq. (11) shows that the wave velocity is determined by the mass density, the second and third order elastic constants of rock, the far-field stresses, the normalized distance $\overline{r} = r/a$ from the borehole surface, and the normalized wave number $k_a = ka$.

4. RESULTS AND DISCUSSIONS

Here we take Barre granite as an example to discuss stress-induced wave-velocity change around the borehole in the natural coordinate. The elastic parameters of Barre granite is shown in Table I, where the velocities of longitudinal and shear waves for Barre granite free of stress are 3790 *m/s* and 2621 *m/s*.

Table I The elastic parameters of Barre granite [4]

Rock	$\rho\left(kg/m^3\right)$	$\lambda(GPa)$	$\mu(GPa)$	$l(GPa)$	$m(GPa)$	$n(GPa)$
Barrre granite	2650	1.67	18.2	−3371	−6742	−6600

Fig.2 shows the relation between the wave-velocity change and the normalized wave number k_a at $\sigma_{11} = -5$ MPa, $\sigma_{22} = -10$ MPa, $\sigma_{33} = -5$ MPa, $\theta = 0^o$, and $\overline{r}$ =1. $\overline{r}$ =1 indicates the borehole surface. The polarizations of P wave, S_1 wave, and S_2 wave are along the axial, radial, and tangential direction of the borehole, respectively. It indicates that the P wave and the S_1 wave are dispersive. We attribute it to the constraint of borehole surface. With the increase of k_a, the velocities of P wave and S_1 wave approach to the constants, which are denoted by the dashed lines in Fig.2, respectively. When $k_a > 2$, the velocities of P wave and S_1 wave could be considered to be constant. In the practical ultrasonic measurement, the frequency of ultrasonic wave is 1MHz, and the hole radius is 2 cm, which corresponds to $k_a > 20$ for common rocks. No constraint in the tangential direction of borehole surface makes S_2 wave non-dispersive, which means that wave frequency has no influence on S_2 wave velocity.

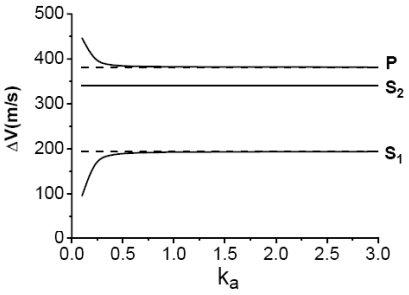

Fig.2 the wave-velocity change and the normalized wave number k_a at $\sigma_{11} = \sigma_{33} = -5$ MPa, $\sigma_{22} = 2\sigma_{11}$, $\theta = 0^o$, and $\overline{r} = 1$.

Fig.3 shows the wave velocity distribution around the borehole surface versus the far-field stress σ_{11} when $\sigma_{11} = \sigma_{22}$, $\sigma_{33} = 0$ MPa, $\overline{r} = 1$, and $k_a = 10$. Fig.3 (a), (b), and (c) correspond to P wave, S_1 wave, and S_2 wave, respectively. Wave velocities increases as the far-field stress σ_{11} increases. The equality of σ_{11} and σ_{22} yields no influence of borehole azimuth on the wave velocities. It is also shown that the derivative of S_2-wave velocity to the far-field stress is greater than that of S_1 wave, which is attributed to that non-zero compressive tangential stress and zero radial stress at the borehole surface give rise to the large tangential stiffness relative to radial stiffness.

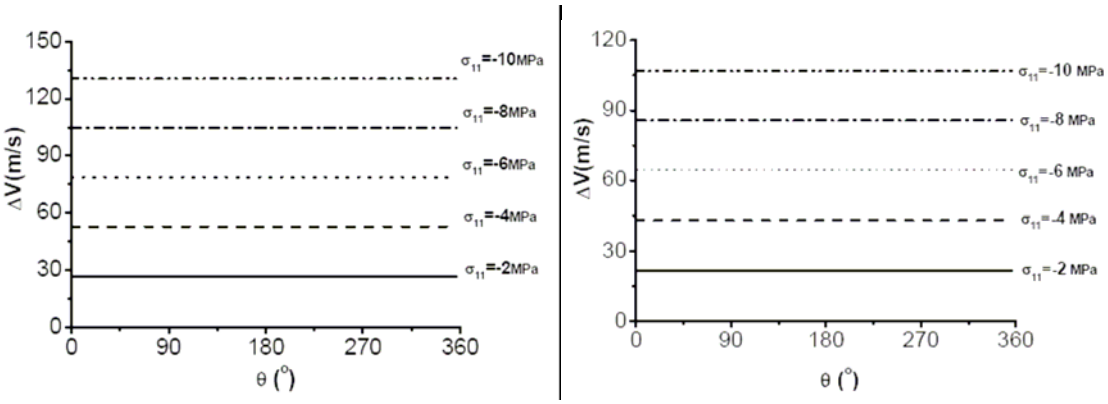

(a) P wave　　（b）S_1 wave

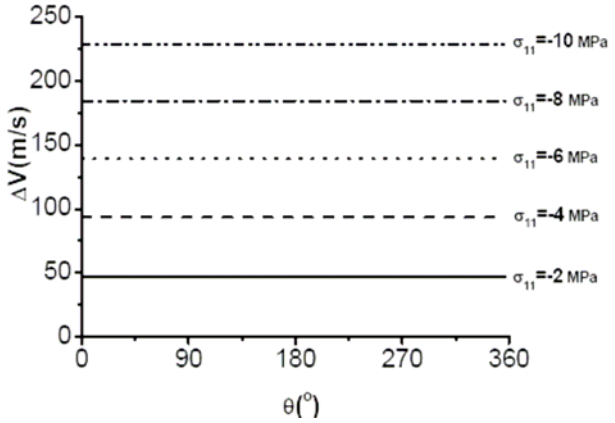

（c）S_2 wave

Fig.3 The relation between the velocity-change distribution around the borehole surface and the far-field stress σ_{11} when $\sigma_{11}=\sigma_{22}$, $\sigma_{33}=0$ MPa, $\bar{r}=1$, and $k_a=10$.(a) P wave, (b) S_1 wave (c) S_2 wave.

Fig.4 shows the wave velocity distribution around the borehole surface when $\sigma_{11}=\sigma_{22}/2$, $\sigma_{33}=0$ MPa, $\bar{r}=1$, and $k_a=10$. It is shown that inequality of two horizontal principal stresses yields the velocity-change versus the borehole azimuth θ as $a\cos(\theta)^2+b$, where a and b are determined by the elastic parameters of rocks and the far-field principal stresses. The azimuth angles corresponding to the local minimum and maximum of velocity change are consistent with the maximal and minimal far-field principal stresses. The measured in-situ stress data show that the maximal horizontal principal stress is approximately two times of the minimal horizontal principal stress. Hence, it is very important to simply determine the direction of the horizontal principal stresses from the minimum and maximum of the measured velocity distribution around the borehole.

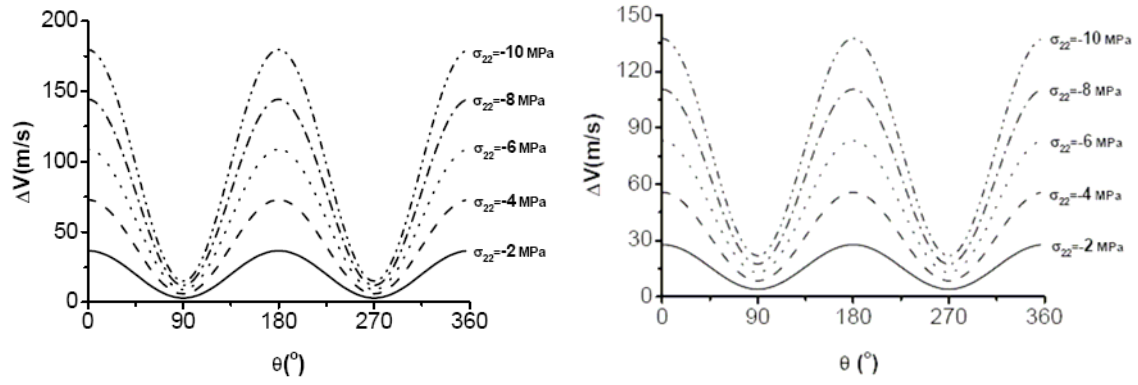

（a）P wave　　（b）S_1 wave

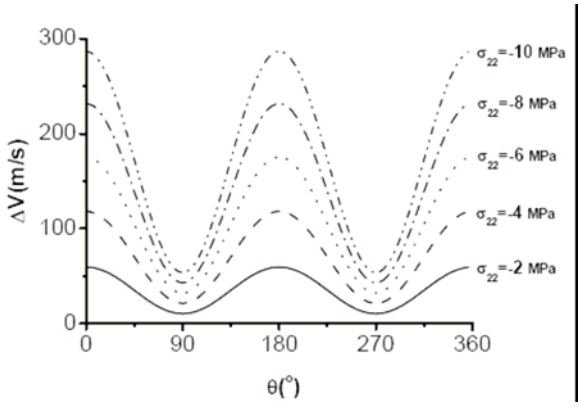

（c） S_2 wave

Fig.4 The velocity-change distribution around the borehole surface when $\sigma_{11} = \sigma_{22}/2$, $\sigma_{33} = 0$ MPa, $\overline{r} = 1$, and $k_a = 10$. (a) P wave, (b) S_1 wave, (c) S_2 wave.

5. EXPERIMENTS

In order to verify the above-mentioned theoretical analysis, the pulse-echo method was used to measure the stress-induced ultrasound-wave velocity change in sandstone. The Figure 5 shows the measurement setup schematically. A hole of radius 2 cm was drilled at the center of sand-rock plate of $20cm \times 20cm \times 3cm$ along z direction. The in-plane biaxial loading is exerted on the rock sample. The longitudinal-wave and normal-incidence shear-wave piezoelectric transducers of 1 MHz were attached on one surface of rock sample, which were arranged near the hole at a certain angle interval. The polarizations of shear wave transducers are along the radial and tangential direction of the hole, respectively. High-power RF pulse transmits by ultrasonic transducer into the rock sample, propagates through the rock sample, reflects from the opposite surface and is received by the same transducer. Measurements of the time delay between reflected echoes, which did not include the influence of the couplant, yields high-resolution wave velocity.

Fig.6 shows the measured velocity-change distribution around the borehole of sandstone at σ_1=15.7MPa and σ_2=7.85MPa. Figs. 6(a), (b), and (c) correspond to P wave, S_1 wave, and S_2 wave, respectively. The measurements for P wave and S_2 wave appear consistent with the theoretical results, except S_1 wave. The measurement for S_1 wave is a little smaller than the theoretical analysis, but they have the similar trend of wave velocity change to the azimuth angle. We attribute it to the constraint and scattering of the borehole surface to the radial vibration.

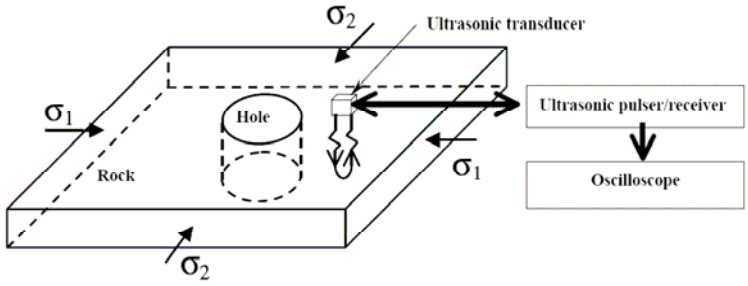

Fig.5 The measurement setup of pulse echo technique

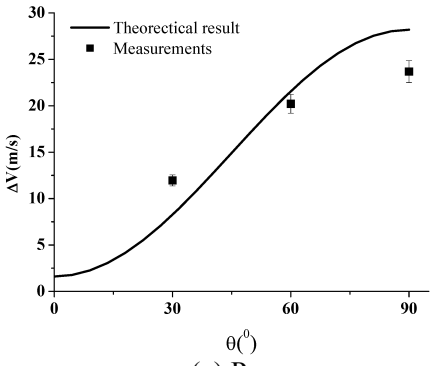

(a) P wave

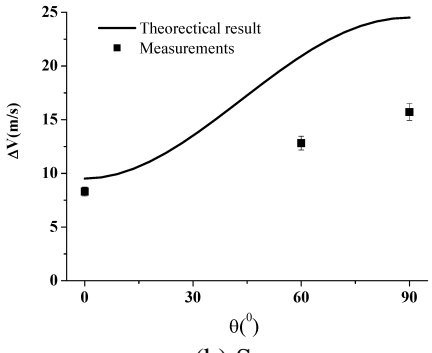

(b) S_1 wave

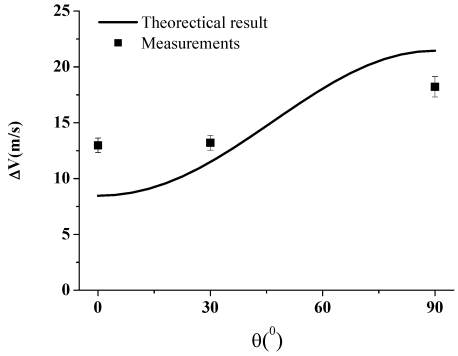

(c) S_2 wave

Fig.6 The measured velocity-change distribution around the borehole of sandstone at $\sigma_1 = 15.70MPa$ and $\sigma_2 = 7.85MPa$

6. CONCLUSIONS

In this paper, we introduce acoustoelasticity theory to investigate quantitative acoustoelastic relation around a borehole in the prestressed rocks. Numerical analysis shows that the azimuth angles corresponding to the local minimum and maximum of velocity change are consistent with the maximal and minimal far-field principal stresses, which s very important to simply determine the direction of the horizontal principal stresses from the minimum and maximum of the measured velocity distribution around the borehole. The pulse-echo measurements for sandstone is consistent with the results of theoretical analysis, which promises that the ultrasonic method based on acoustoelasticity theory could be a promising measurement method of in-situ rock stresses.

ACKNOWLEDGEMENTS

We gratefully acknowledge the support from the National Natural Science Foundation of China (No. 10602053) and research grants from Institute of Crustal Dynamics (No. ZDJ2007-2 and ZDJ2007-28).

APPENDIX: Coefficients in Eq.(11)

$$S_{11} = \sigma_s R_{11sa} + \sigma_d R_{11da} + \sigma_{33} R_{1133} + R_{110},\ S_{12} = \sigma_s R_{12sa} + \sigma_d R_{12da} + \sigma_{33} R_{1233} + R_{120},\ S_{13} = \sigma_d R_{13da}$$

$$S_{21} = \sigma_s R_{21sa} + \sigma_d R_{21da} + \sigma_{33} R_{2133} + R_{210},\ S_{22} = \sigma_s R_{22sa} + \sigma_d R_{22da} + \sigma_{33} R_{2233} + R_{220},\ S_{23} = \sigma_d R_{23da}$$

$$S_{31} = \sigma_d R_{31da},\ S_{32} = \sigma_d R_{32da},\ S_{33} = \sigma_s R_{33sa} + \sigma_d R_{33da} + \sigma_{33} R_{3333} + R_{330},$$

$$\sigma_s = (\sigma_{11} + \sigma_{22})/2,\ \sigma_d = (\sigma_{11} - \sigma_{22})/2$$

$$R_{11sa} = \frac{(\lambda n\bar{r}^2 + 3\lambda n - 4\lambda\mu\bar{r}^2 + 12\lambda\mu - 8\mu^2\bar{r}^2 - 8m\mu\bar{r}^2 + 2n\mu\bar{r}^2 + 2n\mu + 8\mu^2)\cos(\theta)}{4\bar{r}^2\mu^2(3\lambda + 2\mu)}$$

$$R_{11da} = \frac{1}{4(\lambda+\mu)\mu^2\bar{r}^4}\left[\begin{array}{l}(-4\lambda\mu\bar{r}^4 + 4\lambda\mu\bar{r}^2 - 4\mu^2\bar{r}^4 - n\mu\bar{r}^4 + 4m\mu\bar{r}^2 - \lambda n\bar{r}^4 + 4\mu^2\bar{r}^2 - n\bar{r}^2\mu)\cos(\theta) + \\ (4m\mu\bar{r}^2 + 12\lambda\mu\bar{r}^2 + 12\mu^2\bar{r}^2 + 2\lambda n\bar{r}^2 - 12\lambda\mu + n\bar{r}^2\mu - 12\mu^2 - 3n\mu - 3\lambda n)\cos(3\theta)\end{array}\right]$$

$$R_{1133} = -R_{2233} = \frac{(\lambda n + 8\lambda\mu + 8\mu^2 + 4m\mu)\cos(\theta)}{4(3\lambda + 2\mu)\mu^2},\quad R_{11d} = R_{22d} = -R_{110} = -R_{220} = \cos(\theta)$$

$$R_{12sa} = \frac{(-3\lambda n + \lambda n\bar{r}^2 - 12\lambda\mu - 4\lambda\mu\bar{r}^2 - 2n\mu - 8\mu^2\bar{r}^2 - 8\mu^2 - 8m\mu\bar{r}^2 + 2n\mu\bar{r}^2)\sin(\theta)}{4\bar{r}^2\mu^2(3\lambda + 2\mu)}$$

$$R_{12da} = \frac{1}{4(\lambda+\mu)\mu^2\bar{r}^4}\left[\begin{array}{l}(4\lambda\mu\bar{r}^4 + \lambda n\bar{r}^4 + 4\lambda\mu\bar{r}^2 - n\bar{r}^2\mu + 4m\mu\bar{r}^2 + 4\mu^2\bar{r}^4 + 4\mu^2\bar{r}^2 + n\mu\bar{r}^4)\sin(\theta) + \\ (4\lambda\mu\bar{r}^2 - 3\lambda n - 12\lambda\mu + 2\lambda n\bar{r}^2 + 3n\bar{r}^2\mu - 3n\mu - 12\mu^2 + 4\mu^2\bar{r}^2 - 4m\mu\bar{r}^2)\sin(3\theta)\end{array}\right]$$

$$R_{1233} = R_{2133} = \frac{(\lambda n + 8\lambda\mu + 8\mu^2 + 4m\mu)\sin(\theta)}{4(3\lambda + 2\mu)\mu^2}, \quad R_{12d} = -R_{21d} = -R_{120} = R_{210} = -\sin(\theta)$$

$$R_{13da} = \frac{2I(-2\lambda^2 - 2\lambda m + \lambda n - 2\lambda\mu + 2n\mu - 4m\mu + 4l\mu)\cos(3\theta)}{(\lambda + \mu)\mu^2 k_a \bar{r}^3}$$

$$R_{21sa} = \frac{(\lambda n\bar{r}^2 + 3\lambda n - 4\lambda\mu\bar{r}^2 + 12\lambda\mu - 8\mu^2\bar{r}^2 - 8m\mu\bar{r}^2 + 2n\mu + 2n\mu\bar{r}^2 + 8\mu^2)\sin(\theta)}{4\bar{r}^2\mu^2(3\lambda + 2\mu)}$$

$$R_{21da} = \frac{1}{4(\lambda + \mu)\mu^2\bar{r}^4}\left[\begin{array}{l}(n\bar{r}^2\mu + \lambda n\bar{r}^4 - 4\lambda\mu\bar{r}^2 - 4\mu^2\bar{r}^2 + n\mu\bar{r}^4 + 4\mu^2\bar{r}^4 + 4\lambda\mu\bar{r}^4 - 4m\mu\bar{r}^2)\sin(\theta) + \\ (4m\mu\bar{r}^2 + 12\lambda\mu\bar{r}^2 + 12\mu^2\bar{r}^2 + 2\lambda n\bar{r}^2 + n\bar{r}^2\mu - 12\mu^2 - 12\lambda\mu - 3n\mu - 3\lambda n)\sin(3\theta)\end{array}\right]$$

$$R_{22sa} = \frac{(-3\lambda n + \lambda n\bar{r}^2 - 12\lambda\mu - 4\lambda\mu\bar{r}^2 - 2n\mu - 8\mu^2\bar{r}^2 - 8\mu^2 - 8m\mu\bar{r}^2 + 2n\mu\bar{r}^2)\cos(\theta)}{4\bar{r}^2\mu^2(3\lambda + 2\mu)}$$

$$R_{22da} = \frac{1}{4(\lambda + \mu)\mu^2\bar{r}^4}\left[\begin{array}{l}(4\lambda\mu\bar{r}^4 + \lambda n\bar{r}^4 + 4\lambda\mu\bar{r}^2 - n\bar{r}^2\mu + 4m\mu\bar{r}^2 + 4\mu^2\bar{r}^4 + 4\mu^2\bar{r}^2 + n\mu\bar{r}^4)\sin(\theta) + \\ (-2\lambda n\bar{r}^2 - 4\lambda\mu\bar{r}^2 + 12\mu^2 + 4m\mu\bar{r}^2 + 12\lambda\mu + 3\lambda n - 3n\bar{r}^2\mu - 4\mu^2\bar{r}^2 + 3n\mu)\sin(3\theta)\end{array}\right]$$

$$R_{23da} = \frac{2I(-2\lambda^2 - 2\lambda m + \lambda n - 2\lambda\mu + 2n\mu - 4m\mu + 4l\mu)\sin(3\theta)}{(\lambda + \mu)\mu^2 k_a \bar{r}^3}$$

$$R_{31da} = -\frac{I(\lambda n + 4\lambda\mu - 4m\mu + 2n\mu + 4\mu^2)\cos(2\theta)}{(\lambda + \mu)\mu^2 k_a \bar{r}^3}, \quad R_{32da} = -\frac{I(\lambda n + 4\lambda\mu - 4m\mu + 2n\mu + 4\mu^2)\sin(2\theta)}{(\lambda + \mu)\mu^2 k_a \bar{r}^3}$$

$$R_{33sa} = -\frac{2(-\lambda^2 - 2\lambda\mu - 2\lambda m + 2l\mu)}{\mu^2(3\lambda + 2\mu)}, \quad R_{33da} = \frac{2(\lambda + 2l)\cos(2\theta)}{(\lambda + \mu)\mu\bar{r}^2}$$

$$R_{3333} = -\frac{2\lambda^2 + 9\lambda\mu + 4\lambda m + 4m\mu + 2l\mu + 6\mu^2}{(3\lambda + 2\mu)\mu^2}, \quad R_{33d} = 1, \quad R_{330} = -\frac{\lambda + 2\mu}{\mu}$$

REFERENCES

1. Pao, Y.H., Sachse, W., and H. Fukuoka (1984). Acoustoelasticity and ultrasonic measurements of residual stresses, *Physical Acoustics*,(Mason, W. P., Thurston, R.N. ed.) **17**: 61-143. Academic Press, New York, USA.
2. Hirao, M. and Ogi, H. (2003). EMATs for science and industry: Noncontacting ultrasonic measurements, Kluwer, Boston, USA.
3. Nur, A. and Simmons, G. (1969). Stress-induced velocity anisotropy in rock, *Journal of Geophysical Research*, **74**, 6667-6674
4. Johnson, P. and Rasolofosaon, P. (1996), Nonlinear elasticity and stress-induced anisotropy in Rock, *Journal of Geophysical Research*, **101**:3113-3124.
5. Huang, X., Burns, D.R., and Toksoez, M.N.(2002). The effect of stresses on sound velocity in rocks: The theory of acoustoelasticity and experimental measurements, MIT reports, MIT, USA.
6. Vega, S. (2004). Intrinsic and stress-induced velocity anisotropy in unconsolidated sands, Ph.D. thesis, Stanford University, USA.
7. Winkler, K.W., Sinha, B.K., and Plona, T.J. (1998). Effects of borehole stress concentrations on dipole anisotropy measurements, *Geophysics* **63** (1): 11-17.
8. Sinha, B.K., Papanastasiou, P., and Plona, T.J.(1997), Influence of triaxial stresses on borehole Stoneley and flexural dispersions, *Expanded Abstracts, 67th SEG Annual International Meeting and Exposition*, paper BH2.2, Dallas, Texas, USA.
9. Su, K.Z.(1985). Measurement of crustal stress, Seismic Press, Beijing, China.(In Chinese)
10. Cai, M.F., et al (1995). Measurement principle and technology of crustal stress, Science Press, Beijing, China. (In Chinese)
11. Murnaghan, T.D. (1951). Finite deformation of an elastic solid, John Wiley and Sons Inc., New York, USA.